A FRAMEWORK FOR WAVELET-BASED ANALYSIS AND PROCESSING OF COLOR FILTER ARRAY IMAGES WITH APPLICATIONS TO DENOISING AND DEMOSAICING

Keigo Hirakawa, Xiao-Li Meng, and Patrick J. Wolfe

Harvard University
Department of Statistics
Division of Engineering and Applied Sciences
Oxford Street, Cambridge, MA 02138 USA
{hirakawa,meng,wolfe}@stat.harvard.edu

ABSTRACT

This paper presents a new approach to demosaicing of spatially sampled image data observed through a color filter array, in which properties of Smith-Barnwell filterbanks are employed to exploit the correlation of color components in order to reconstruct a subsampled image. The method is shown to be amenable to wavelet-domain denoising prior to demosaicing, and a general framework for applying existing image denoising algorithms to color filter array data is also described. Results indicate that the proposed method performs on a par with the state of the art for far lower computational cost, and provides a versatile, effective, and low-complexity solution to the problem of interpolating color filter array data observed in noise.

Index Terms— Wavelets, CFA Image, Demosaicing, Denoising

1. INTRODUCTION

In digital imaging applications, data are typically obtained via a spatial subsampling procedure implemented as a color filter array (CFA), a physical construction whereby each pixel location measures only a single color. The most well known of these schemes involve the primary colors of light: red, green, and blue. In particular, the Bayer pattern CFA [1], shown in Fig. 3, attempts to complement humans' spatial color sensitivity via a quincunx sampling of the green component that is twice as dense as that of red and blue.

The term *demosaicing* refers to the inverse problem of reconstructing a spatially undersampled vector field whose components correspond to these primary colors. It is well known that the optimal solution to this ill-posed inverse problem, in the L^2 sense of an orthogonal projection onto the space of bandlimited functions separately for each spatially subsampled color channel, produces unacceptable visual distortions and artifacts.

Aside from the spatial undersampling inherent in the Bayer pattern, this phenomenon can be attributed to the observation that values of the color triple exhibit significant correlation, particularly at high spatial frequencies: such content often signifies the presence of edges, whereas low-frequency information contributes to distinctly perceived color content. As such, most demosaicing algorithms described in the literature attempt to make use (either implicitly or explicity) of this correlation structure in the spatial frequency domain.

A wavelet-based method of decorrelating these components, for the purposes of efficient lossless color image compression, was recently proposed by Zhang *et al.* [2]. Here we conceive an alternative motivation for this type of wavelet analysis of CFA images, according to fundamental principles of Fourier analysis and filterbanks.

This structure admits a new framework for wavelet-based CFA image denoising and demosaicing methods, which in turn enables the application of existing wavelet-based image denoising techniques directly to sparsely sampled data. This capability is important owing to the fact that various noise sources inherent to the charge-coupled device or other imaging technique employed must be taken into account in practice; any noise reduction procedure should ideally take place prior to demosaicing (both to improve interpolation results and to avoid introducing additional correlation structure into the noise). While earlier work has been focused primarily on demosaicing prior to denoising, the method we propose suggests a natural way to perform wavelet-based denoising and demosaicing together in tandem.

2. SPECTRAL ANALYSIS OF CFA IMAGES

We first re-cast the demosaicing problem in light of the observation in [2] that the CFA image may be viewed as the sum of a fully observed green pixel array and sparsely sampled *difference images* corresponding to red and blue. Specifically, let $\boldsymbol{n} = \begin{bmatrix} n_0 & n_1 \end{bmatrix}^T$ index pixel location and define $\boldsymbol{x}(\boldsymbol{n}) = \begin{bmatrix} \boldsymbol{r}(\boldsymbol{n}) & \boldsymbol{g}(\boldsymbol{n}) & \boldsymbol{b}(\boldsymbol{n}) \end{bmatrix}^T$ to be the corresponding color triple. If we define difference images $\boldsymbol{\alpha}(\boldsymbol{n}) = \boldsymbol{r}(\boldsymbol{n}) - \boldsymbol{g}(\boldsymbol{n})$ and $\boldsymbol{\beta}(\boldsymbol{n}) = \boldsymbol{b}(\boldsymbol{n}) - \boldsymbol{g}(\boldsymbol{n})$, then the CFA image is given by $\boldsymbol{y}(\boldsymbol{n}) = \boldsymbol{g}(\boldsymbol{n}) + \boldsymbol{\alpha}_s(\boldsymbol{n}) + \boldsymbol{\beta}_s(\boldsymbol{n})$, where

$$\boldsymbol{\alpha}_s(\boldsymbol{n}) := \begin{cases} \boldsymbol{r}(\boldsymbol{n}) - \boldsymbol{g}(\boldsymbol{n}) & \text{if } n_0, n_1 \text{ even} \\ 0 & \text{otherwise} \end{cases}$$

$$\boldsymbol{\beta}_s(\boldsymbol{n}) := \begin{cases} \boldsymbol{b}(\boldsymbol{n}) - \boldsymbol{g}(\boldsymbol{n}) & \text{if } n_0, n_1 \text{ odd} \\ 0 & \text{otherwise} \end{cases}$$

are the sparsely sampled difference images.

The fact that difference channels $\boldsymbol{\alpha}(\boldsymbol{n})$ and $\boldsymbol{\beta}(\boldsymbol{n})$ exhibit rapid spectral decay relative to the green channel $\boldsymbol{g}(\boldsymbol{n})$ follows from the (de-)correlation of color content at high frequencies, as explained in Section 1. This result is well known [3], and may be observed empirically in Fig. 1(a)-(c), which show the log-magnitude spectra of $\boldsymbol{g}(\boldsymbol{n}), \boldsymbol{\alpha}(\boldsymbol{n}), \boldsymbol{\beta}(\boldsymbol{n})$, respectively denoted by $\boldsymbol{G}(\boldsymbol{\omega}), \boldsymbol{A}(\boldsymbol{\omega}), \boldsymbol{B}(\boldsymbol{\omega})$ for frequency variable $\boldsymbol{\omega} = \begin{bmatrix} \omega_0 & \omega_1 \end{bmatrix}^T$.

It follows from the composition of the dyadic decimation and interpolation operators induced by the Bayer sampling pattern that the Fourier transform $\boldsymbol{Y}(\boldsymbol{\omega})$ of $\boldsymbol{y}(\boldsymbol{n}) = \boldsymbol{g}(\boldsymbol{n}) + \boldsymbol{\alpha}_s(\boldsymbol{n}) + \boldsymbol{\beta}_s(\boldsymbol{n})$ is

$$\boldsymbol{Y}(\boldsymbol{\omega}) = \boldsymbol{G}(\boldsymbol{\omega}) + \frac{1}{4} \sum_{k_0,k_1=0}^{1} \boldsymbol{A}(\boldsymbol{\omega} + \pi\boldsymbol{k}) + (-1)^{k_0+k_1} \boldsymbol{B}(\boldsymbol{\omega} + \pi\boldsymbol{k}).$$
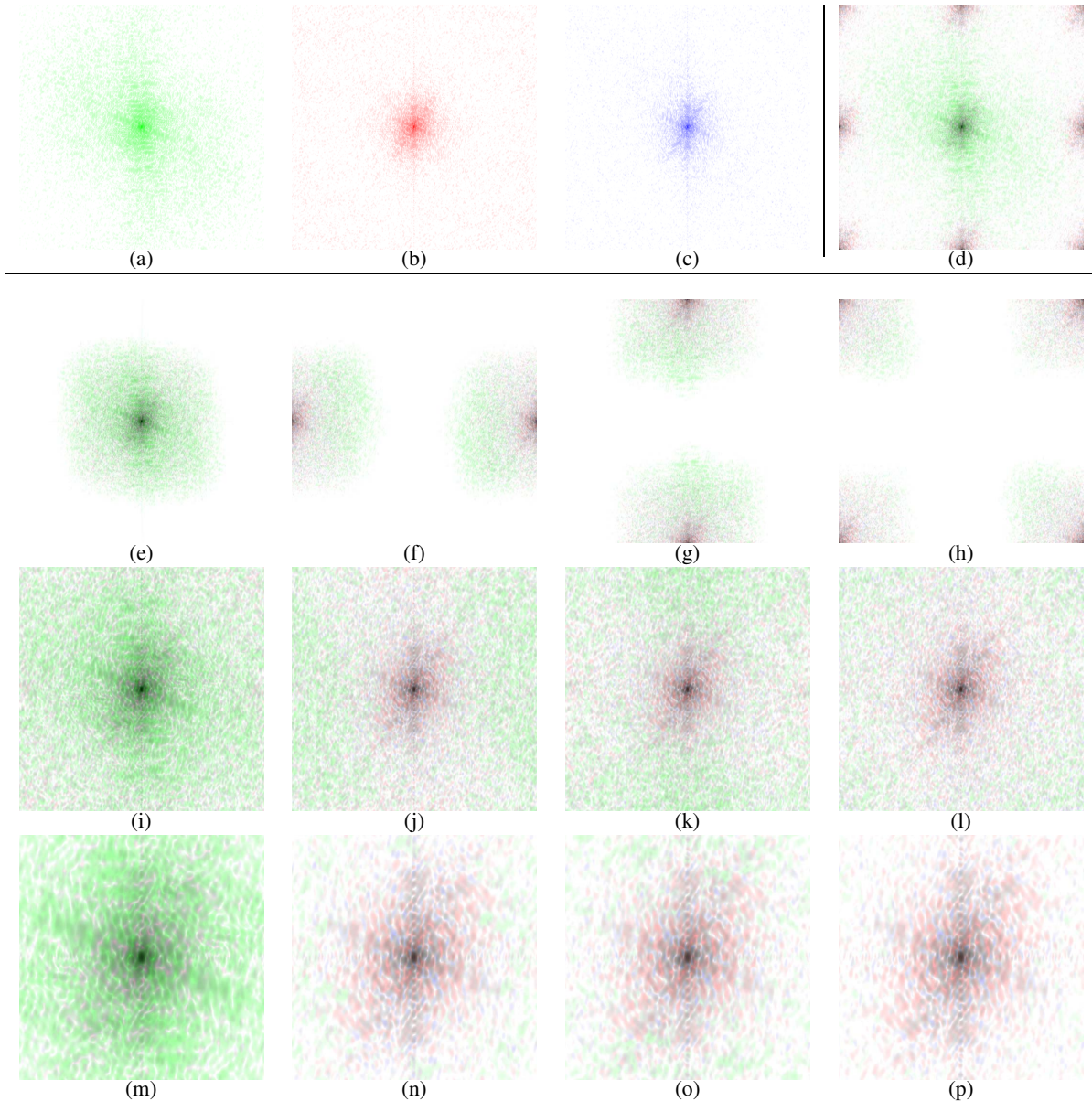
Fig. 1. Log-magnitude spectra of a typical color image ("Clown"), with $g(n)$ component shown in green, $\alpha(n) = r(n) - g(n)$ component in red, and $\beta(n) = b(n) - g(n)$ component in blue. Plots (a)–(c) in the first row show the green and difference channel log-magnitude spectra corresponding to (a) $G(\omega)$, (b) $A(\omega)$, (c) $B(\omega)$; plot (d) shows that of the CFA data corresponding to $Y(\omega)$. Plots (e)–(h) in the second row show the result of directional filtering as (e) $H_{LL}(\omega)Y(\omega)$, (f) $H_{LH}(\omega)Y(\omega)$, (g) $H_{HL}(\omega)Y(\omega)$, (h) $H_{HH}(\omega)Y(\omega)$; plots (i)–(l) in the third row show the corresponding result of subsequent dyadic decimation. The final row of plots (m)–(p) show the result of an additional wavelet decomposition of each subband shown immediately above, corresponding to lowpass filtering via H_{LL} and subsequent decimation. According to their phases (not visible here), appropriate linear combinations of (n)–(p) enable the separation of red and blue color content.

Figure 1(d) shows $Y(\omega)$ represented as a sum of $g(n)$ (green), $\alpha_s(n)$ (red), and $\beta_s(n)$ (blue). Note that the rectangular subsampling lattice shifts the spectral content of $\alpha(n)$ and $\beta(n)$ ("aliasing"), and also induces spectral copies centered about the set of frequencies $\omega \in \{(0, \pi), (\pi, 0), (\pi, \pi)\}$ ("imaging").

In fact, it is possible to take advantage of the lowpass nature of these subsampled difference signals to separate the color components of data observed through a color filter array, as we now detail. Recall that a separable wavelet transform is equivalent to a set of convolutions corresponding to directional filtering in two dimen-

sions, followed by a separable dyadic decimation about both spatial frequency axes. The application of these steps to $y(n)$ is detailed in the second row of Fig. 1, which shows the log-magnitude spectrum after filtering according to the standard directional wavelet filterbank low- and highpass transfer functions $H_{LL}(\omega)$, $H_{HL}(\omega)$, $H_{LH}(\omega)$, and $H_{HH}(\omega)$, respectively, and the third row of Fig. 1, which shows the result of subsequent decimation.

The composition of these operators is equivalent to a remapping of each color channel's spatial frequency content to the origin, and a subsequent dilation of each spectrum. In particular, assum-
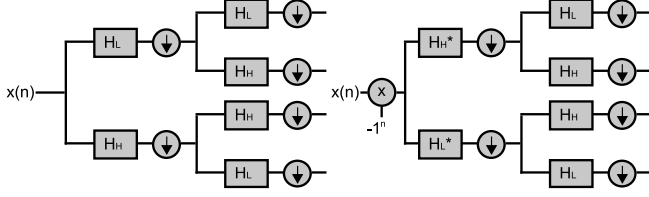
Fig. 2. Equivalent filterbanks for $\gamma(n)$.

(a)   (b)   (c)

Fig. 3. Portion of test data: (a) original "Clown" image, (b) CFA image, (c) noisy CFA image ($\sigma^2 = 625$).

ing that the spectral content of the difference channels is sufficiently low relative to that of the green channel, this operation provides a method for effectively separating the spectral energy of individual color components, as shown in the final row of Fig. 1 (see caption).

3. WAVELET ANALYSIS OF SUBSAMPLED SEQUENCES

Suppose that, as in the case of Daubechies wavelets, the directional transfer functions $\{\boldsymbol{H}_{\text{LL}}, \boldsymbol{H}_{\text{LH}}, \boldsymbol{H}_{\text{HL}}, \boldsymbol{H}_{\text{HH}}\}$ introduced in Section 2 comprise a filterbank satisfying the Smith-Barnwell (S-B) condition. In this case, the subsampled difference images $\boldsymbol{\alpha}_s(\boldsymbol{n})$ and $\boldsymbol{\beta}_s(\boldsymbol{n})$ may be conveniently represented in the wavelet domain as follows.[1]

Let $\{\boldsymbol{H}_{\text{L}}(\omega), \boldsymbol{H}_{\text{H}}(\omega)\}$ be a S-B filter pair such that $\boldsymbol{H}_{\text{H}}(\omega) = -e^{-j\omega m}\boldsymbol{H}_{\text{L}}(-\omega + \pi)$, where m is an odd integer, and let $d_i \in \{\text{L}, \text{H}\}$ index the filter passband of the decomposition at level i. If we consider a sequence $\boldsymbol{\gamma}(n)$ and its corresponding even-subsampled version $\boldsymbol{\gamma}_s(n) := \frac{1}{2}[\boldsymbol{\gamma}(n) + (-1)^n\boldsymbol{\gamma}(n)]$, then the first-level filter-bank decomposition of $\boldsymbol{\gamma}_s(n)$, denoted $\boldsymbol{W}_{d_1}(\omega)$, is equivalent to the sum of the corresponding decompositions of $\boldsymbol{\gamma}(n)$ and $(-1)^n\boldsymbol{\gamma}(n)$ (denoted $\frac{1}{2}\boldsymbol{W}'_{d_1}(\omega)$ and $\frac{1}{2}\boldsymbol{W}''_{d_1}(\omega)$, respectively). These decompositions in turn are related to the spectrum $\boldsymbol{\Gamma}(\omega)$ of $\boldsymbol{\gamma}(n)$ as

$$\boldsymbol{W}'_{d_1}(\omega) = \frac{1}{2}\left[\boldsymbol{H}_{d_1}\left(\frac{\omega}{2}\right)\boldsymbol{\Gamma}\left(\frac{\omega}{2}\right) + \boldsymbol{H}_{d_1}\left(\frac{\omega}{2} + \pi\right)\boldsymbol{\Gamma}\left(\frac{\omega}{2} + \pi\right)\right]$$

$$\boldsymbol{W}''_{d_1}(\omega) = \frac{1}{2}\left[\boldsymbol{H}_{d_1}\left(\frac{\omega}{2} + \pi\right)\boldsymbol{\Gamma}\left(\frac{\omega}{2}\right) + \boldsymbol{H}_{d_1}\left(\frac{\omega}{2}\right)\boldsymbol{\Gamma}\left(\frac{\omega}{2} + \pi\right)\right]$$

$$= c_{d_1}\frac{\omega}{4}\left[\boldsymbol{H}^*_{d_1^{-1}}\left(\frac{\omega}{2}\right)\boldsymbol{\Gamma}\left(\frac{\omega}{2}\right) + \boldsymbol{H}^*_{d_1^{-1}}\left(\frac{\omega}{2} + \pi\right)\boldsymbol{\Gamma}\left(\frac{\omega}{2} + \pi\right)\right],$$

where $\cdot^*$ denotes the complex conjugate, and we have the following for m odd:

$$d_1^{-1} = \begin{cases} \text{H} & \text{if } d_1 = \text{L} \\ \text{L} & \text{if } d_1 = \text{H} \end{cases}, \quad c_{d_1}(\omega) = \begin{cases} e^{j\omega m} & \text{if } d_1 = \text{L} \\ -e^{-j\omega m} & \text{if } d_1 = \text{H} \end{cases}.$$

For the case of the Haar wavelet, we have $\boldsymbol{H}_{d_1} = c_{d_1}\boldsymbol{H}^*_{d_1}$, and hence by construction the scaling coefficient of $(-1)^n\boldsymbol{\gamma}(n)$ is exactly equal to the wavelet coefficient of $\boldsymbol{\gamma}(n)$, and vice-versa. It follows that the multi-level wavelet decomposition of $(-1)^n\boldsymbol{\gamma}(n)$ is equivalent to the same multi-level wavelet packet decomposition of $\boldsymbol{\gamma}(n)$, but in the reverse order of coarseness to fineness. An example of this filterbank structure equivalence is shown in Fig. 2.

4. WAVELET-BASED CFA IMAGE DEMOSAICING

In addition to providing a natural way to recover the spectra associated with individual color components of a given CFA image $\boldsymbol{y}(\boldsymbol{n})$, the filterbank decomposition of Section 3 also admits a simple formula for reconstructing the complete (i.e., non-subsampled) image $\boldsymbol{x}(\boldsymbol{n})$. Let $\boldsymbol{w}^y_{d_1,d_2}, \boldsymbol{w}^g_{d_1,d_2}, \boldsymbol{w}^\alpha_{d_1,d_2}, \boldsymbol{w}^\beta_{d_1,d_2}$ be the two-level wavelet (packet) transforms via S-B filterbanks of $\boldsymbol{y}(\boldsymbol{n}), \boldsymbol{g}(\boldsymbol{n}), \boldsymbol{\alpha}(\boldsymbol{n}), \boldsymbol{\beta}(\boldsymbol{n})$, respectively, where d_1, d_2 indicates the filter orientation. Then (as may be seen from the example of Fig. 1, particularly Fig. 1(d)), if

---

[1]For clarity of exposition, we consider only the univariate case here; the extension to two dimensions is straightforward.
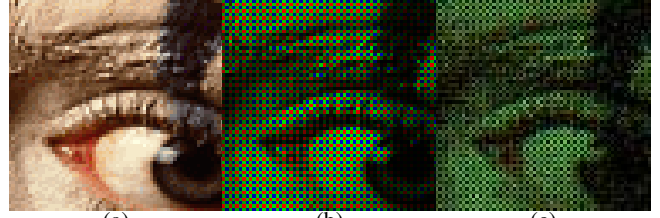
the spectral content of the difference channels is sufficiently low-pass with respect to that of the green color channel, the following approximations will be accurate:

$$\begin{aligned}\boldsymbol{w}^y_{\text{LL,LL}} =& \boldsymbol{w}^g_{\text{LL,LL}} + \frac{1}{4}[\boldsymbol{w}^\alpha_{\text{LL,LL}} + \boldsymbol{w}^\alpha_{\tilde{\text{LH}},\text{LL}} + \boldsymbol{w}^\alpha_{\tilde{\text{HL}},\text{LL}} + \boldsymbol{w}^\alpha_{\tilde{\text{HH}},\text{LL}}] \\ &+ \frac{1}{4}[\boldsymbol{w}^\beta_{\text{LL,LL}} - \boldsymbol{w}^\beta_{\tilde{\text{LH}},\text{LL}} - \boldsymbol{w}^\beta_{\tilde{\text{HL}},\text{LL}} + \boldsymbol{w}^\beta_{\tilde{\text{HH}},\text{LL}}] \\ \approx& \boldsymbol{w}^g_{\text{LL,LL}} + \frac{1}{4}\boldsymbol{w}^\alpha_{\text{LL,LL}} + \frac{1}{4}\boldsymbol{w}^\beta_{\text{LL,LL}}, \end{aligned} \quad (1)$$

where $\tilde{\cdot}$ denotes reversal of a sequence. Similarly,

$$\boldsymbol{w}^y_{\tilde{\text{LH}},\text{LL}} \approx \boldsymbol{w}^y_{\tilde{\text{HL}},\text{LL}} \approx \frac{1}{4}[\boldsymbol{w}^\beta_{\text{LL,LL}} - \boldsymbol{w}^\alpha_{\text{LL,LL}}] \quad (2)$$

$$\boldsymbol{w}^y_{\tilde{\text{HH}},\text{LL}} \approx \frac{1}{4}[\boldsymbol{w}^\alpha_{\text{LL,LL}} + \boldsymbol{w}^\beta_{\text{LL,LL}}]. \quad (3)$$

Assuming that these approximations hold, $\boldsymbol{x}(n)$ may then be recovered from its wavelet coefficients as follows:

$$\hat{\boldsymbol{w}}^g_{d_1,d_2} = \begin{cases} \boldsymbol{w}^y_{\text{LL,LL}} - \boldsymbol{w}^y_{\tilde{\text{HH}},\text{LL}} & \text{if } d_1 = d_2 = \text{LL} \\ \boldsymbol{w}^y_{d_1,d_2} & \text{if } d_2 \neq \text{LL} \\ 0 & \text{otherwise} \end{cases} \quad (4)$$

$$\hat{\boldsymbol{w}}^\alpha_{d_1,d_2} = \begin{cases} 2\boldsymbol{w}^y_{\tilde{\text{HH}},\text{LL}} - \boldsymbol{w}^y_{\tilde{\text{LH}},\text{LL}} - \boldsymbol{w}^y_{\tilde{\text{HL}},\text{LL}} & \text{if } d_1 = d_2 = \text{LL} \\ 0 & \text{otherwise} \end{cases}$$

$$\hat{\boldsymbol{w}}^\beta_{d_1,d_2} = \begin{cases} 2\boldsymbol{w}^y_{\tilde{\text{HH}},\text{LL}} + \boldsymbol{w}^y_{\tilde{\text{LH}},\text{LL}} + \boldsymbol{w}^y_{\tilde{\text{HL}},\text{LL}} & \text{if } d_1 = d_2 = \text{LL} \\ 0 & \text{otherwise} \end{cases}.$$

5. WAVELET-BASED CFA IMAGE DENOISING

Wavelet-based methods for image denoising have proved immensely popular in the literature, in part because the resultant shrinkage or thresholding estimators $\hat{\boldsymbol{w}}$ are simple and computationally efficient, yet they may enjoy excellent theoretical properties and adapt well to spatial inhomogeneities. However, as far as the authors are aware, typical techniques to date have been designed for grayscale or complete color image data, and hence must be applied *after* demosaicing.

It is possible to model noisy difference images in the wavelet domain directly, within the statistical framework of missing data, though the computational burden of doing so is severe [6]. However, the arguments put forth in preceding sections regarding the spectral content of CFA images suggest a much simpler scheme as follows.

First, note that when $d_2 \neq \text{LL}$, it can be expected that the wavelet coefficients $\hat{\boldsymbol{w}}$ estimated by some shrinkage operator will satisfy the relationship $\hat{\boldsymbol{w}}^g_{d_1,d_2} \approx \hat{\boldsymbol{w}}^y_{d_1,d_2}$. Furthermore, (1) implies that $\boldsymbol{w}^y_{\text{LL,LL}}$ represents the $\{\text{LL}, \text{LL}\}$ subband coefficients of

$$\boldsymbol{g}(\boldsymbol{n}) + \frac{1}{4}\boldsymbol{\alpha}(\boldsymbol{n}) + \frac{1}{4}\boldsymbol{\beta}(\boldsymbol{n}) = \frac{1}{2}\boldsymbol{g}(\boldsymbol{n}) + \frac{1}{4}\boldsymbol{r}(\boldsymbol{n}) + \frac{1}{4}\boldsymbol{b}(\boldsymbol{n}),$$

which provides a means of estimating an image's luminance component (which in turn exhibits statistics similar to a grayscale image).
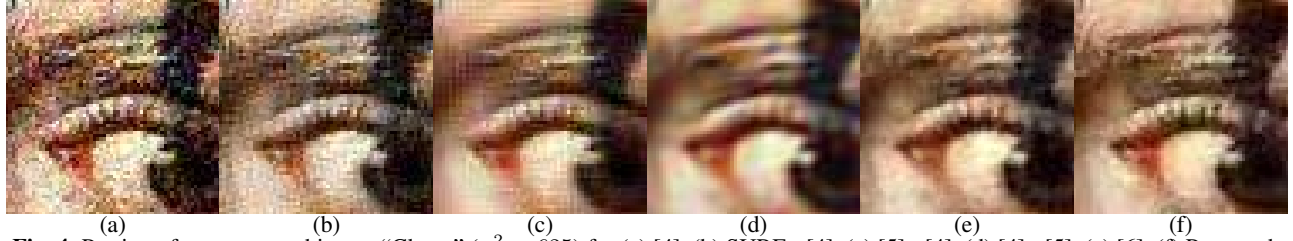
Fig. 4. Portion of reconstructed image "Clown" ($\sigma^2 = 625$) for (a) [4], (b) SURE+ [4], (c) [5]+ [4], (d) [4]+ [5], (e) [6], (f) Proposed.

Table 1. CFA image denoising evaluated using MSE.

Method	Clown		Lena	
	$\sigma^2 = 100$	$\sigma^2 = 625$	$\sigma^2 = 100$	$\sigma^2 = 625$
SURE	80.04	349.47	84.34	446.39
[5]	55.35	164.42	34.44	91.12
Proposed	50.04	141.10	29.31	92.71

Table 2. Denoising+demosaicing evaluated using SCIELAB.

Method	Clown		Lena	
	$\sigma^2 = 0$	$\sigma^2 = 625$	$\sigma^2 = 0$	$\sigma^2 = 625$
[4]	14.52	242.97	1.45	46.02
SURE+ [4]	–	255.21	–	59.52
[5]+ [4]	–	155.07	–	32.40
[4]+ [5]	–	218.18	–	20.26
[6]	12.70	132.53	1.13	18.47
Proposed	19.91	135.46	2.25	19.52

Thus, we may consider obtaining $\hat{w}_{\text{LL,LL}}^y$ via a standard denoising strategy. Finally, the quantities of (2) and (3) correspond to {LL, LL} subband coefficients from the difference images $r(n) - b(n)$ and $\alpha(n) + \beta(n)$. As smoothed approximate versions of images themselves, they too are likely to be amenable to standard wavelet-based denoising algorithms.

6. EXPERIMENTAL RESULTS

In order to test the proposed denoising and demosaicing schemes for CFA data, both separately as well as in tandem, a variety of numerical experiments was performed using widely available test images commonly referred to as "Clown" and "Lena." These images were first subsampled according to the Bayer pattern and then corrupted with additive white Gaussian noise of mean zero (Fig. 3). Reconstruction methods were implemented using separable Daubechies wavelets, with cycle-spinning employed for the first-level decomposition, and the nondecimated wavelet transform for the subsequent.

First, the corrupted data were used to compare the performance of three wavelet-based algorithms for denoising: the SURE Shrink method of [7] applied independently to each wavelet coefficient; a model based on scale mixtures of Gaussians [5] applied to each of the de-interlaced color channels of the CFA image in turn; and the proposed implementation of Section 5 using the wavelet coefficient model of [6]. Denoising was performed using a total of three decomposition levels and a shrinkage operator described in [6], with the noise variance σ^2 estimated from the {HH, HH} subband as in [8]. Table 1 compares the mean-square error (MSE) of the various denoised CFA images.

By treating the denoised output $\hat{w}_{d_1,d_2}^y$ as input to the demosaicing algorithm proposed in Section 4, a method of combined denoising and demosaicing was obtained and subsequently tested. Table 2 shows the average SCIELAB distance [9] of the output images from the original input images for the proposed method as well as several alternatives, and Fig. 4 shows a portion of the various reconstructions. Performance of the proposed technique is comparable to [6] but with significantly reduced computational cost; it also improves noticeably upon the noise observed in Figs. 4(a) and (b), and offers enhanced edge preservation relative to alternatives that treat denoising and demosaicing separately, as shown in Figs. 4(c) and (d).

7. CONCLUSION

This paper introduced a framework for wavelet-based color image analysis and processing, in which properties of Smith-Barnwell filterbanks were employed to exploit the correlation structure of color components in order to reconstruct a subsampled CFA image. In addition to yielding new algorithms for denoising and demosaicing, this framework was also shown to enable the application of other wavelet-based denoising algorithms directly to the CFA image data. Results indicate that the proposed methods perform on a par with the state of the art for far lower computational cost, and provide a versatile, effective, and low-complexity solution to the problem of interpolating color filter array data observed in noise. A particular topic of future work will be to extend this methodology to allow for the optimization of wavelet-based compression schemes in conjunction with denoising and demosaicing of CFA data.

8. REFERENCES

[1] B. E. Bayer, "Color imaging array," US Patent 3 971 065, 1976.

[2] N. Zhang and X. Wu, "Lossless compression of color mosaic images," *IEEE Trans. Image Processing*, vol. 15, no. 6, pp. 1379–1388, June 2006.

[3] B. K. Gunturk, J. Glotzbach, Y. Altunbasak, R. W. Schafer, and R. M. Mersereau, "Demosaicking: Color filter array interpolation in single chip digital cameras," *IEEE Signal Processing Magazine*, vol. 22, no. 1, pp. 44–54, January 2005.

[4] B. K. Gunturk, Y. Altunbasak, and R. M. Mersereau, "Color plane interpolation using alternating projections," *IEEE Trans. Image Processing*, vol. 11, no. 9, pp. 997–1013, September 2002.

[5] J. Portilla, V. Strela, M. J. Wainwright, and E. P. Simoncelli, "Image denoising using scale mixture of Gaussians in the wavelet domain," *IEEE Trans. Image Processing*, vol. 12, no. 11, pp. 1338–1351, November 2003.

[6] K. Hirakawa and X.-L. Meng, "An empirical Bayes EM-wavelet unification for simultaneous denoising, interpolation, and/or demosaicing," *IEEE Int'l Conf Image Processing*, October 2006.

[7] David L. Donoho and Iain M. Johnstone, "Adapting to unknown smoothness via wavelet shrinkage," *Journal of the American Statistical Association*, vol. 90, no. 432, pp. 1200–1224, 1995.

[8] S. B. Chang, B. Yu, and M. Vetterli, "Spatially adaptive wavelet thresholding with context modeling for image denoising," *IEEE Trans. Image Processing*, vol. 9, no. 9, pp. 1522–1531, 2000.

[9] X. Zhang and B. Wandell, "A spatial extension of CIELAB for digital color image reproduction," *Proc. Soc. Inform. Display 96 Digest*, pp. 731–734, 1996.